

51

# A System for 3D Carotid Characterization from Magnetic Resonance and Histology Data

by

Ana Gabriela Isasi

B.S., Chemical Engineering (1999)  
B.S., Mathematics (1999)  
Massachusetts Institute of Technology

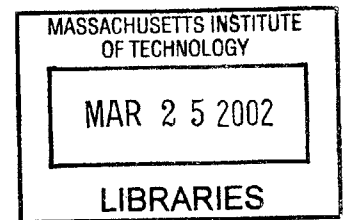
Submitted to the Department of Mechanical Engineering  
in Partial Fulfillment of the Requirements  
for the Degree of

Master of Science  
in Mechanical Engineering

at the

Massachusetts Institute of Technology  
February 2002

**BARKER**



© 2002 Massachusetts Institute of Technology  
All rights reserved

Signature of Author.....  
Department of Mechanical Engineering  
September 10, 2001

Certified by.....  
Roger D. Kamm  
Professor of Mechanical Engineering and BEH  
Thesis Supervisor

Accepted by.....  
Ain A. Sonin  
Chairman, Departmental Committee on Graduate Studies  
Department of Mechanical Engineering

# **A System for 3D Carotid Characterization from Magnetic Resonance and Histology Data**

by

Ana Gabriela Isasi

Submitted to the Department of Mechanical Engineering on September 10, 2001  
in Partial Fulfillment of the Requirements for the

Degree of Master of Science in Mechanical Engineering

## **Abstract**

Atherosclerosis is known to be associated with the stresses that act on or within the arterial wall. Still, the uneven distribution of atherosclerotic lesions within the arterial tree is poorly understood. It has been hypothesized that these distributional differences can be explained by the occurrence of low fluid dynamic shear stress at certain locations, which has been shown to correlate well with areas of disease. The aim of this study is to develop methods to construct a model that can be used to test this hypothesis.

A technique for the 3D reconstruction of the vascular geometry and the velocity distribution in the carotid bifurcation in vivo from geometry and velocity magnetic resonance (MR) images of atherosclerotic patients that will undergo carotid endarterectomy (AP) was developed. To this end, novel edge detection algorithms implemented in computer programs (written using Matlab<sup>TM</sup>), software capable of easy visualization and interpolation (Tecplot<sup>TM</sup>) and finite element modeling (FEM) software (ADINA<sup>TM</sup>) were used. The resulting model, together with the fluid and wall properties, can be inputted into FEM software to obtain shear stress and principal stress distributions in the carotid bifurcation, from fluid dynamics, wall mechanics and fluid-solid interaction (FSI) FEM simulations.

To complement the geometry and velocity data, the chemical composition of the atherosclerotic plaque lining the carotid bifurcation was determined. This was done quantitatively using image processing software (OPTIMAS<sup>TM</sup>), using sections of the excised specimen that were stained for macrophages, collagen, smooth muscle cells (SMC's) and lipids. A semi-automated computer routine that will build a 3D histological model of the atherosclerotic plaque is currently being developed.

**Keywords:** Atherosclerosis, MR, carotid bifurcation, arterial wall stress, low/oscillatory shear stress, 3D reconstruction, FEM, edge detection, carotid endarterectomy, 3D histological model.

Thesis Supervisor: Roger D. Kamm, Ph.D.  
Title: Professor of Mechanical Engineering

## Acknowledgements

I would like to thank Professor Roger Kamm for his unconditional support, patience and guidance during the preparation for the doctoral qualifying examinations and the research year that preceded this thesis. His knowledge and integrity, together with his lively sense of humor, are making my graduate school experience at MIT rewarding, both from an intellectual and human perspective. I thank him for engaging individuals of very diverse backgrounds in the research group, making it friendly and interesting.

It is in the Fluids Lab that I have made unique friendships as a graduate student. Over late night talks in the lab, Belinda Yap, Nikola Kojic, and Arpita Upadhyaya have listened uncomplainingly to my frustrations with research and life in general at MIT, providing me with the support and optimism I needed, specially during the rough times.

I have been lucky to find in Dr Ray Chan both, a source of encouragement, and an image-processing guru. At some point, when there is more currency in my bank account, he will receive the half a dozen ponies I owe him. I thank Hesham Younis for being a source of inspiration and for his great salads.

Dr Galina Sukhova's and Eugenia Shvartz beautiful histology stains, together with their hilarious wit and their inquiring about my family in Uruguay, made my trips to Brigham and Womens' in the middle of the day, carrying freshly excised specimens, an experience to look forward to. I always had a smile on my face when leaving their lab.

Dr Denise Hinton's contribution to the study scanning AP's and NV's, and her modifying innumerable times the scanning protocol to accommodate the research team's and the patients' needs, has been invaluable. Her cheerful approach to research subjects and her infinite patience in the magnet room have made it a pleasure to work with her.

I want to thank UROP student Linda Kim for generously contributing most of her free time during the past year to the steady progress of this project. Research volunteer Deepa Santhumayar spent long hours photographing and reconstructing histology stained slivers. Dr Chanil Chung was very helpful in the initial stages of research. Dr Mohammad R. K-Mofrad worked on the FEM that uses as input the results from this study. UROP students Lucia Contreras, Alyx Chau, Yuki Hori and Teresa Kim worked hard on different parts of the project. I want to thank the MGH surgeons Dr. Cambria, Dr Gertler and Dr Lamuraglia, as well as their administrative staff, for collaborating in this study. Dr Rich Lee's guidance with histology quantification was invaluable, and Dr Robert Lees and Dr Fred Holmvang greatly expedited my accessing patients' ultrasounds at MGH.

I want to thank my hostmother in Boston, Kate Baty, for her generous love and care during difficult times. I am thankful to my friends Carlos, Moni and Mimi, and to my Abuela Marina and my brother Alvaro in Uruguay, for their continuous support via email and through the phone, which has remained uninterrupted over the past six years.

Finally, I want to express complete gratitude, love and respect to my parents Susana and Eduardo. They have known my weaknesses, strengths and dreams for the past 25 years, and still continue to respect my freedom, to have the uttermost confidence in my reaching the goals I set for myself, and to love me unconditionally. They taught me what is important, and how to fight for it. They opened the initial window from which I could see where I wanted to go. They then gave me the initial push to help me climb onto the windowsill. Once I had climbed, they told me to fly, and have continued doing so ever since. Most importantly, they taught me that absolutely nothing in life is impossible.

## Table of Contents

Title Page .....	1
Abstract .....	2
Acknowledgements .....	3
Table of Contents .....	4
Introduction .....	5
Methods and Results .....	7
1. Overall Strategy.....	7
2. MR Imaging.....	8
3. Extraction of Inner and Outer Wall coordinates: 2-step process.....	10
3.1 First Step: Anisotropic Smoothing and edge enhancement.....	10
3.2 Second Step: Contour Extraction.....	12
4. 3D Reconstruction.....	13
5. Construction of the FEM and application of the boundary conditions.....	15
6. Velocity Interpolation and Construction of Time functions.....	16
7. Other specifications needed for the FEM simulation.....	18
8. Histology: Staining.....	19
8.1 First Step: Rationale for choosing these four particular indicators....	19
8.2 Detailed Procedure.....	20
9. Histology: Composition Quantification.....	21
10. Summary of the overall protocol for the study.....	27
Discussion and Recommendations for Future Research.....	28
1. Overall Strategy.....	28
2. MR Imaging.....	29
3. Extraction of Inner and Outer Wall coordinates and 3D Reconstruction.....	30
4. Velocity Interpolation and Construction of Time functions.....	30
5. Histology: Staining.....	32
6. Histology: Composition Quantification.....	33
Conclusion.....	35
References.....	36

## **Introduction**

Atherosclerosis is a geometrically focal inflammatory disease, preferentially affecting the outer edges of vessel bifurcations (Malek, 1999). From a fluid mechanics perspective, it poses a particularly thought-provoking research problem, in that it preferentially affects sites of complex hemodynamics, such as bifurcations, junctions and regions of high curvature (Davies PF, 1988). From an epidemiological viewpoint, atherosclerosis constitutes a challenging problem. This disease affects 70-80 percent of Americans, it is responsible for two thirds of deaths and is often linked to a diet high in saturated fat and cholesterol (Lees, 2001). Even though several systemic risk factors that predispose individuals to atherosclerosis have been identified, these fail to explain the uneven distribution of atherosclerotic lesions within the arterial tree.

Atherosclerosis involves a complex process of lesion inflammation (Ross, 1999). In the initial stages endothelial permeability increases, and there is upregulation of leukocyte adhesion molecules in endothelial cells. This results in leukocyte (primarily monocyte) adhesion to the endothelium of the arterial wall and the eventual migration of leukocytes into the artery wall (Ross, 1993). During the same time, lipids begin to accumulate in the arterial wall, entering via site of cell death and turnover, during which the wall is “leaky” to lipids and other macromolecules. On further progression, foam cells form from differentiated monocytes (this follows monocyte transmigration into the wall) and T-cell activation by the uptake of lipid into the cells. Foam cells together with T lymphocytes constitute what is called a fatty-streak. Next, there is smooth muscle cell migration from within the media layer of the arterial wall into the intimal layer. At this stage in the inflammation process, platelet activation and adherence of platelets to the intimal surface take place. With time, fatty streaks evolve to intermediate and advanced lesions, forming a fibrous cap consisting of leukocytes, lipids and debris, which may form a necrotic core. Plaque fissuring is due to concentrations of circumferential tensile stress on the cap tissue, particularly in plaques containing a soft core of lipid; weakening of cap tissue by an infiltrate of macrophages is a contributory factor (Davies MJ, 1990).

In the early phase of disease, the wall expands outward with little change in luminal dimension. In late stage disease the plaque thickens, narrowing the vessel lumen, causing ischemia. Eventually, if the disease is left untreated, there can be a thinning of the fibrous

cap over a lipid pool, which may lead to a fracture in the wall, with or without the further complication of hemorrhage from the plaque microvessels. This vascular event could in turn cause thrombus formation (clotting), either due to exposure of the passing blood to clotting factors in the wall, or of the small, ruptured, microvessels, either of which could potentially develop into a myocardial infarction (coronary artery) or stroke (carotid artery) (Davies MJ, 1990).

Currently, understanding of the role of hemodynamic shear stress in the development and progression of atherosclerosis is incomplete. The stresses that act on or within the arterial wall affect the inflammation process, as well as the heterogeneous remodeling of the vessel structure and composition (Davies PF, 1993). In the early stages of disease, low or oscillatory fluid shear stresses cause monocyte adhesion and affect endothelial cell function, while high cyclical mechanical strain affects endothelial and smooth muscle cell activity (Sumpio, 1991). In the late stages of atherosclerosis, low or oscillatory fluid shear stress has been shown to correlate with vulnerable areas in the atherosclerotic plaque, such as sections with thin fibrous cap and large lipid pool (Loree, 1992), or regions with a deficit in collagen fibrils (Sukhova, 1999) and a surplus of macrophages (Libby, 1996). It has also been shown that high mechanical strain enhances matrix metalloproteinase (MMP) production by macrophages, potentially causing the plaque cap to weaken. (Lee, 1996)

The methods described in this paper will be used to generate, from MRI *in vivo* data, geometry and velocity files that will in turn be used to carry out numerical simulations that aim to verify the correlations of low shear/high strain regions to sites of inflammation, and high strain regions to locations of stimulated MMP production, that have been shown in previous studies (Lee, 1996).

For the purpose of this study, MR imaging will be used to acquire geometry and velocity *in vivo* data. There are several reasons that make MR imaging an attractive option for data acquisition. MR provides reliable and high-resolution images of vascular structure and flow velocity, as well as it being a non-invasive procedure. Moreover, given that cardiovascular imaging is a relatively new application for MR in routine clinical practice, its clinical monitoring potential as a tool for accurate diagnosis, assessment of

treatment efficacy, clinical decision-making and post-surgery remodeling evaluation, is presently not fully utilized, making breakthrough innovation in that field possible.

The location in the body that was chosen for characterization using the developed methods is the carotid bifurcation. This position in the circulatory system is particularly appealing from a research viewpoint for several reasons. Firstly, the carotid bifurcation is a frequent site of disease amongst atherosclerotic patients, hence guaranteeing the availability of patients for the study. Additionally, the existence of two symmetrical carotid bifurcation sites makes a potential asymmetry study possible. Thirdly, the recurrent nature of plaque formation at this particular site makes analysis of lesion evolution viable. Furthermore, the carotid bifurcation is relatively superficially located, making the positioning of the surface coil for the purpose of imaging a moderately simple task. Yet, the most important reason for having chosen the carotid bifurcation as the subject matter of this study is the fact that the standard treatment for advanced lesions is endarterectomy, hence ensuring the availability of excised specimens for histological staining and quantitative analysis.

## **Methods and Results**

### 1. Overall Strategy

The initial step of the developed process is the acquisition of MR geometry and velocity data of AP's, and of normal volunteers (NV's), using a surface coil that yields 0.39mm in-plane resolution over 2mm thick slices. The purpose of scanning NV's, from whom histology data will not be available, is to develop, and to some extent validate the methods of the analysis. Given that the protocol is lengthy and has numerous stages, each patient dataset is precious. Hence, the developed methods must be tested on data that are more readily available, in order to profit as much as possible from the patient data.

Studying NV's enables the comparison of fluid mechanics' parameters such as shear stress, as calculated in this study, with parameters resulting from ideal geometry simulations that appear in previous publications (Delfino 1996). Apart from providing a means of validation for the developed methods, given that NV geometry is usually

similar to the idealized model of the carotid bifurcation, scanning NV's is a useful tool to get qualitative and semi-quantitative insight into intra-subject variability, and to modify the scanning procedure so as to make it as comfortable and as brief as possible, without sacrificing data quality and thoroughness.

MR imaging is followed by a step-wise process of image analysis, beginning with the application of an edge detection protocol to the geometry MR data. The 3D vascular structure is reconstructed using the modeling software, by lofting across the 2D cross-sectional structures of each level of carotid bifurcation. Next, the obtained geometry is imported into the FEM software, where a mesh is constructed that matches the vessel geometry, and the nodes at the inlet plane to the carotid bifurcation (common carotid), and those of one of the outlet planes to the carotid bifurcation (internal carotid), are extracted. Subsequently, the coordinates of the aforementioned nodes are inputted as arguments into a computer function that interpolates across pixels in the MR velocity data, and returns a file with velocity values for each node. The geometry, velocity at the inlet, and velocity at the outlet files can then be imported into the FEM software, where fluid and wall properties are entered, making it possible to simulate the fluid dynamics, wall mechanics and FSI of *in vivo* data.

Additionally, at the time of endarterectomy, the excised plaque specimen is collected. The sample is then sliced in 5 mm thick slivers, and stained for collagen, macrophages, lipids and SMC's. Apart from providing qualitative information about the plaque composition, the stained samples are analyzed using image-processing software to yield a 2D composition map at each level of the extracted plaque. Currently, a protocol that will use these 2D processed images to obtain a 3D reconstruction of the plaque histology, is being developed using methods similar to those used for the 3D reconstruction of the MR geometry data. This histological 3D model will improve component visualization, simplifying the task of comparing the chemical composition map from the excised histology with the stress distribution *in vivo* from the FEM simulation, in order to investigate the effects of fluid mechanics' parameters such as stress and strain on plaque composition and stability.



## 2. MR Imaging

The 2D MR images are obtained using a Siemens Sonata 1.5 Tesla system that utilizes linear scaling. Denise Hinton, PhD, performs the scans, at the Massachusetts General Hospital NMR Center. The image is encoded using a 16-bit image, with signed integers that take positive and negative values, and a velocity encoding value (VENC) of 1600 mm/s. Positive values of the signed integers range from 0 to +VENC, while negative values go from 0 to -VENC. If the absolute value of the recorded velocity exceeds the VENC, wrap around occurs and the image must be corrected. For this study, experience has shown that no wrap around occurs, either for AP or NV acquisitions, if a VENC value of 1600 mm/s is used. The surface coil yields an in-plane resolution lateral voxel dimension of approximately 0.39 mm, and the slice thickness (voxel height) is set to 2mm.

Regarding the geometry data, 20 slices (20 mm below and 20 mm above the carotid bifurcation) are typically acquired using a spin-echo sequence (dark blood imaging) over the course of 20 cardiac cycles. An ECG is connected to the subject to ensure all images are acquired at the same point in the cardiac cycle. The surface area of the images is 256 by 256 pixels. Typically, the resulting vessel diameter is 20 - 30 pixels while the wall thickness is 2 - 3 pixels. Figure 1 depicts a sketch of the way geometry images are acquired. The imaged region is represented by the volume between any two adjacent horizontal lines.

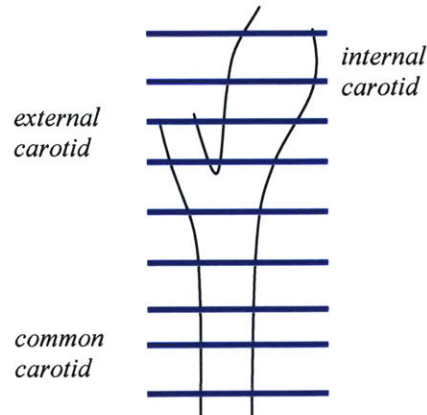


*Figure 1: Acquisition of MR geometry data*

Cross-sectional velocity distribution MR images are acquired for approximately 10 equally-distributed time points throughout cardiac cycle, with a fixed interval between images of 0.078 s, using 2D phase-contrast. These velocity time-functions are obtained for 2 positions in the carotid bifurcation. Position 1 corresponds to the most proximal slice for which geometry data were acquired, at the inlet to the carotid bifurcation, on the common carotid. Position 2 corresponds to the most distal slice for which geometry data were acquired, at the outlet to the carotid bifurcation, comprising both the internal and external carotid arteries. The total procedure lasts about 45 minutes. Figure 2 depicts a sketch of the way cross-sectional velocity images are acquired.

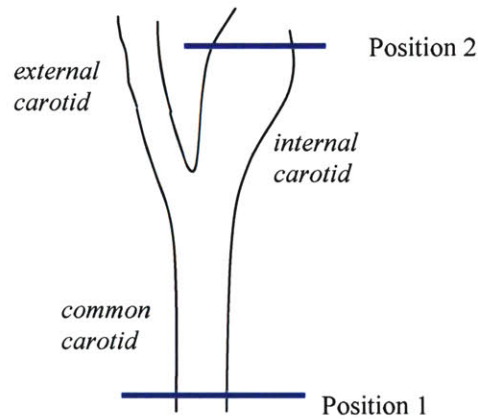


*Figure 2: Acquisition of MR cross-sectional velocity data*

### 3. Extraction of Inner and Outer Wall coordinates : 2-step process

#### 3.1 First Step: Anisotropic smoothing and edge enhancement

The strategy used here for estimating regional vessel structure is based on variational energy minimization and curve evolution (Chan, 2000). A directionally-sensitive segmentation functional allows prior information about arterial shape to be incorporated at each step when delineating region interfaces. In this manner, the level curves of the smoothed image field are coupled with the edge field so that they evolve jointly as the minimization of the functional is performed. Accordingly, stronger gradient penalties are applied to edges that are unaligned with user-specified prior information.

The energy functional that is minimized in the iterations leading to contour extraction is given by equation (1):

$$\hat{f}, \hat{s} = \arg \min_{f,s} \underbrace{\iint \alpha(1-s)^2 \|\nabla_{DS} f\|_1}_{\text{Smoothness\_constraint}} + \underbrace{\beta \|f - g\|_1}_{\text{Data\_fidelity}} + \underbrace{\frac{\rho}{2} \|\nabla_{DS} s\|_2^2 + \frac{s^2}{2\rho}}_{\text{Edge\_penalty}} dx dy \quad (1)$$

In the above equation,  $g(x,y)$  denotes the original image,  $\hat{s}(x,y)$  is the edge field for  $[x,y] \in [0,1]$ ,  $f(x,y)$  is the enhanced image and  $\nabla_{DS}$  is the direction-sensitive gradient. Parameters  $\alpha$ ,  $\beta$  and  $\rho$  affect the evolution of the functional of equation (1) over the original data in different ways. For example, increasing  $\alpha$  makes contours smoother and rounder, while increasing  $\beta$  makes contours follow raw data more closely, resulting in rougher edges due to noise. Similarly, decreasing  $\rho$  makes the image edges thin out. Additionally, the user specifies the boundary direction favored by the direction-sensitive gradient: gradients with the highest positive value are targeted when estimating the outer wall, while gradients with the lowest negative value are the aim when calculating the inner wall boundary. Through the interplay of these parameters, anisotropic smoothing suppresses noise away from edges and makes them more distinct. This step is repeated for each MR geometry cross-sectional image. Figure 3 shows the original MR image, its colormap (the black and white original palette is changed for a color palette for the purpose of clearer visualization), the unwound vessel wall of the colormap, and the final unwound vessel wall after anisotropic smoothing and edge enhancement.

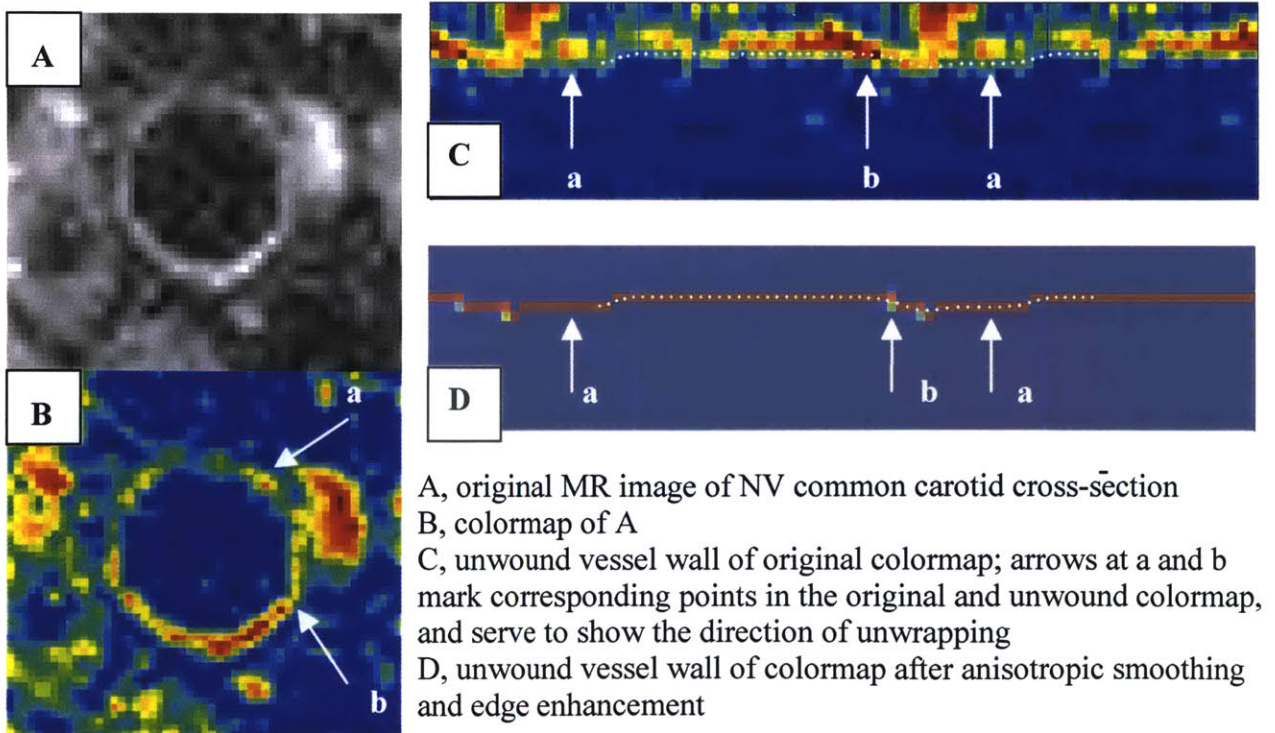


Figure 3: Anisotropic Smoothing and Edge Enhancement

### 3.2 Second Step: Contour Extaction

On the sparse field  $\hat{s}$  obtained in step 1, active contours or *snakes* (Shah, 1996) are evolved into the edges corresponding to the inner (lumen-intima) and outer (media-adventitia) interface boundaries of the carotid artery. A *snake* is a deformable parametric curve that has the form:

$$\vec{v}(t) = [x(t), y(t)], t \in [0, 1] \quad (2)$$

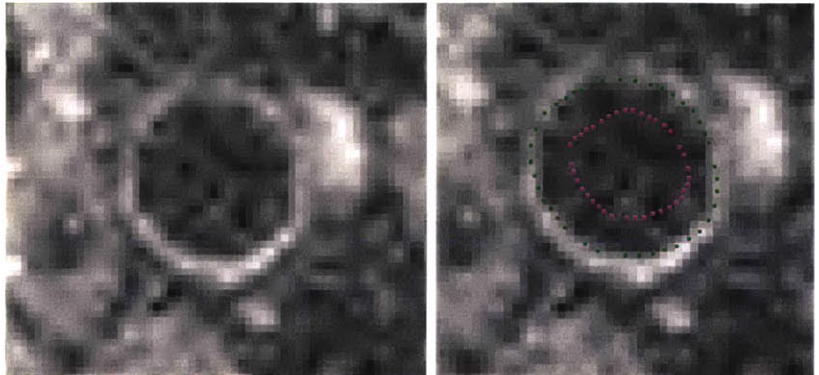
In equation (2),  $t$  is a variable for curve parametrization.

The spline curve  $\vec{v}(t)$  moves over  $\hat{s}(x,y)$ , the edge field for  $[x,y] \in [0, 1]$ , to satisfy:

$$\hat{v} = \arg \min_{\vec{v}} \int_0^1 \underbrace{\frac{1}{2} [a \|\vec{v}'(t)\|_2^2 + b \|\vec{v}''(t)\|_2^2]}_{E_{internal}} - E_{external}(\vec{v}(t)) dt \quad (3)$$

Here,  $a \|\vec{v}'(t)\|_2^2$  is the spline stiffness,  $b \|\vec{v}''(t)\|_2^2$  is the spline rigidity,  $E_{internal}$  is the internal spline energy, and  $E_{external}$  is the external energy from  $\hat{s}$ . The spline is pulled outwards towards the edge  $\hat{s}$  to minimize  $E_{external}$ , and this motion is balanced by the spline smoothness pulling it inwards, aiming to minimize  $E_{internal}$ . The initial contour is that defined at step 1. Following the energy minimization step, the cartesian coordinates of the segmented boundaries are extracted. Once again, this step is repeated for each MR geometry cross-sectional image. Figure 4 depicts an original MR image and its inner wall edge, obtained using the above method. The initial contour (user-specified) is in magenta, while the final contour estimate is in green.

*Figure 4: Original MR image with corresponding user-specified and final inner wall contour. The initial contour (user-specified) is in magenta; the final contour estimate is in green.*



A Matlab function that performs the 2-step process described above, is repeated for each successive carotid cross-section, to yield the set of contours depicted in Figure 5.

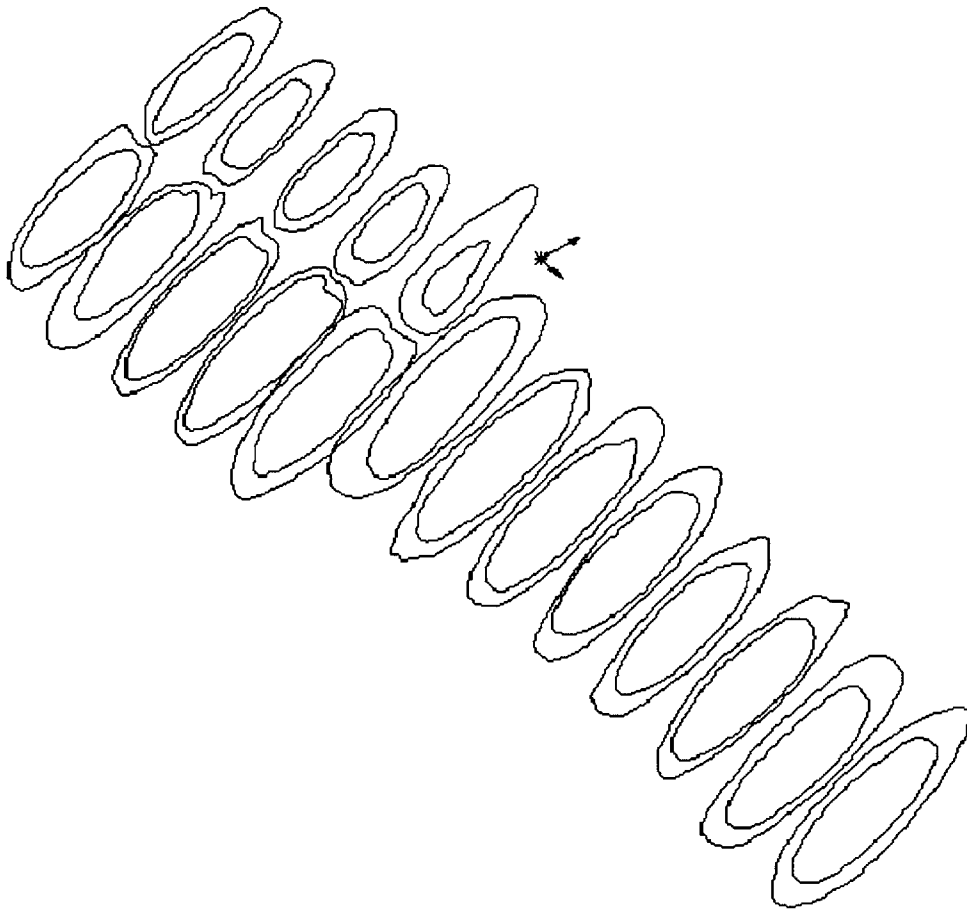


*Figure 5: Set of inner and outer wall edges resulting from the 2-step process*

#### 4. 3D Reconstruction

The curves resulting from the method described in section 3 are subsequently analyzed using the modeling software, where a base loft function interpolates across the 2D cross-sectional structures at each level of the carotid bifurcation, in order to yield 3D structures. The solid that results from interpolating across the outer contours constitutes the outer wall 3D solid body, while the 3D structure that results from interpolating across the inner contours produces the 3D fluid volume. Next, the fluid volume is subtracted from the outer wall volume, hollowing out the 3D outer wall solid body and yielding the

arterial wall 3D solid structure. Figures 6 and 7 depict a sample set of fluid and wall geometries, for a NV and an AP, respectively.

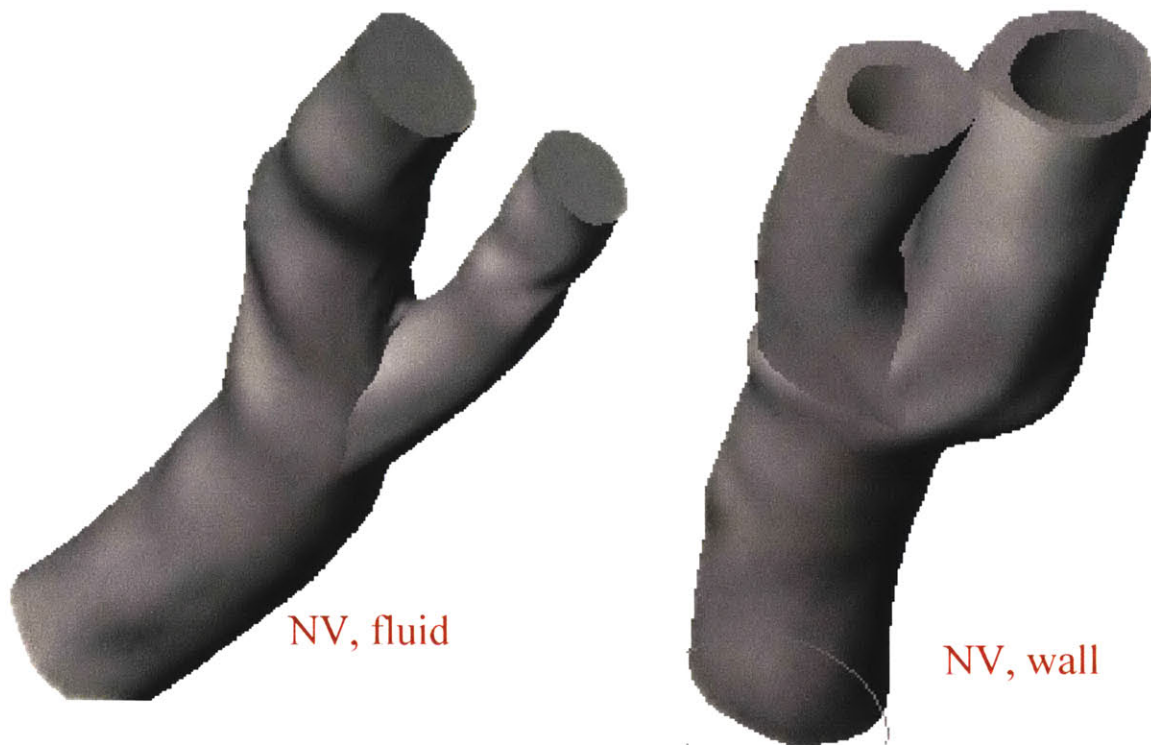


*Figure 6: Fluid and wall geometry for NV resulting from 3D reconstruction*

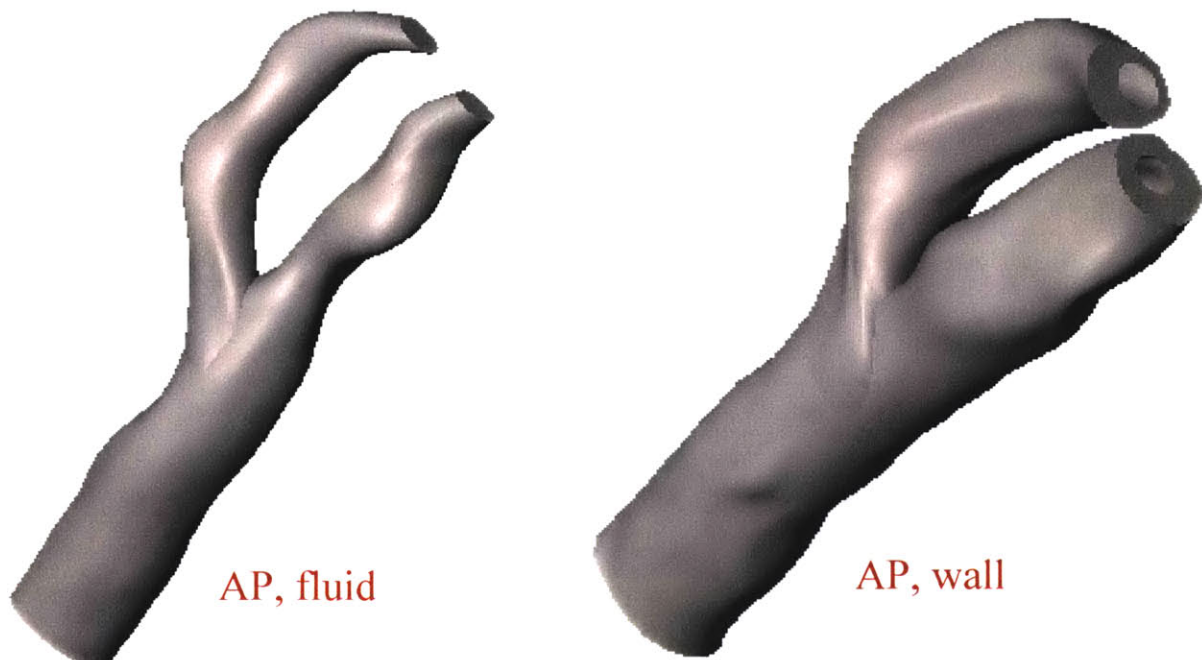


*Figure 7: Fluid and wall geometry for AP resulting from 3D reconstruction*

## 5. Construction of the FEM and application of the boundary conditions

At this point, the 3D fluid and wall geometries that were obtained using the modeling software are transferred to the FEM software. These two structures are then converted into 3D FEM volumes made up of a free mesh that uses 4-node 3D tetrahedral elements. An element length of 0.4mm is used for the fluid, while the element length in the wall is set to 0.5 mm (note that the solid elements are second order, and can therefore be larger than in the fluid, which contains linear elements, and still yield good accuracy). As a result, the fluid FEM has approximately 25,000 nodes and 130,000 elements. Figures 8 and 9 depict a sample set of fluid and wall FEM's, for a NV and an AP, respectively.

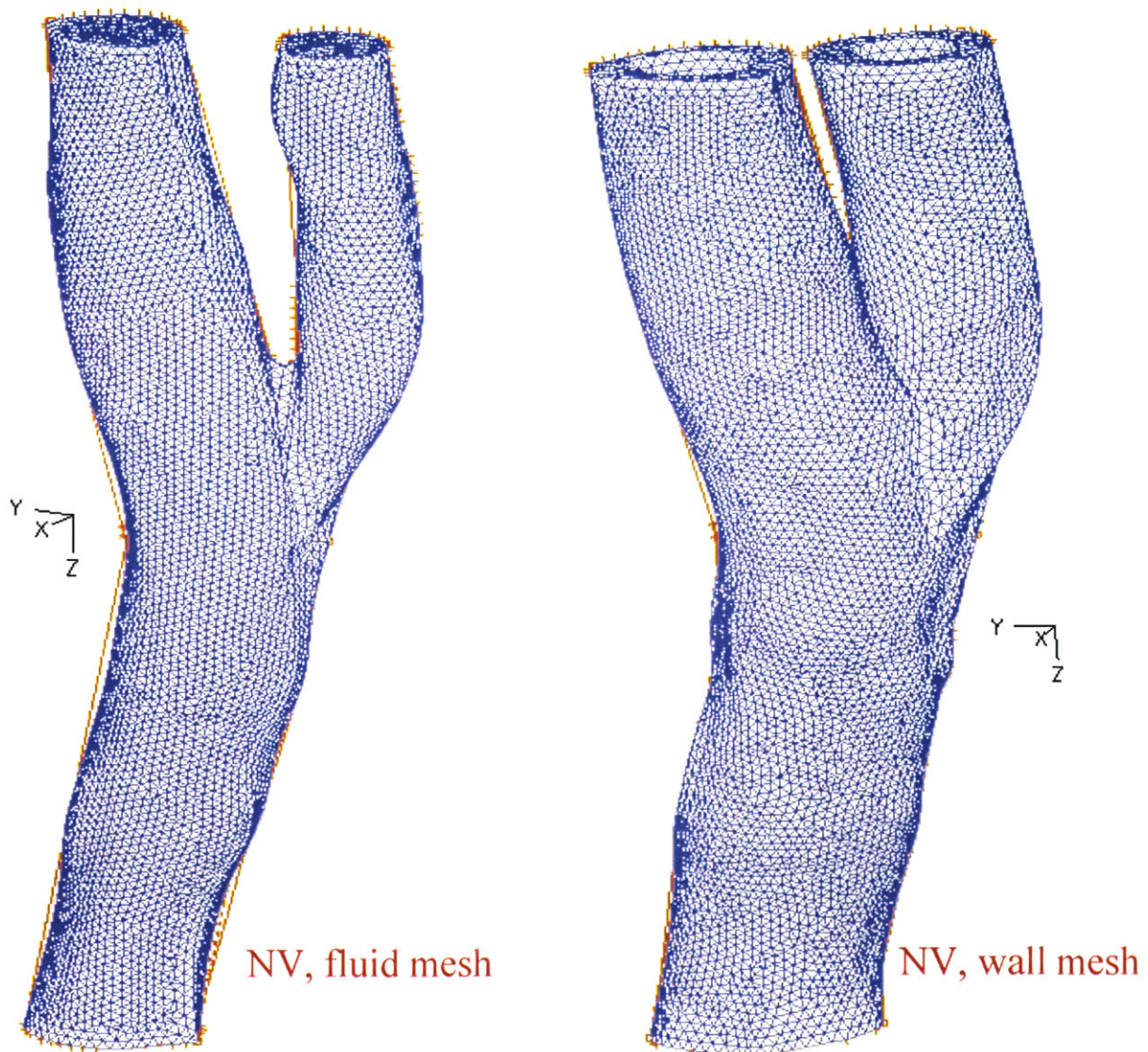


*Figure 8: Fluid and wall FEM for NV*

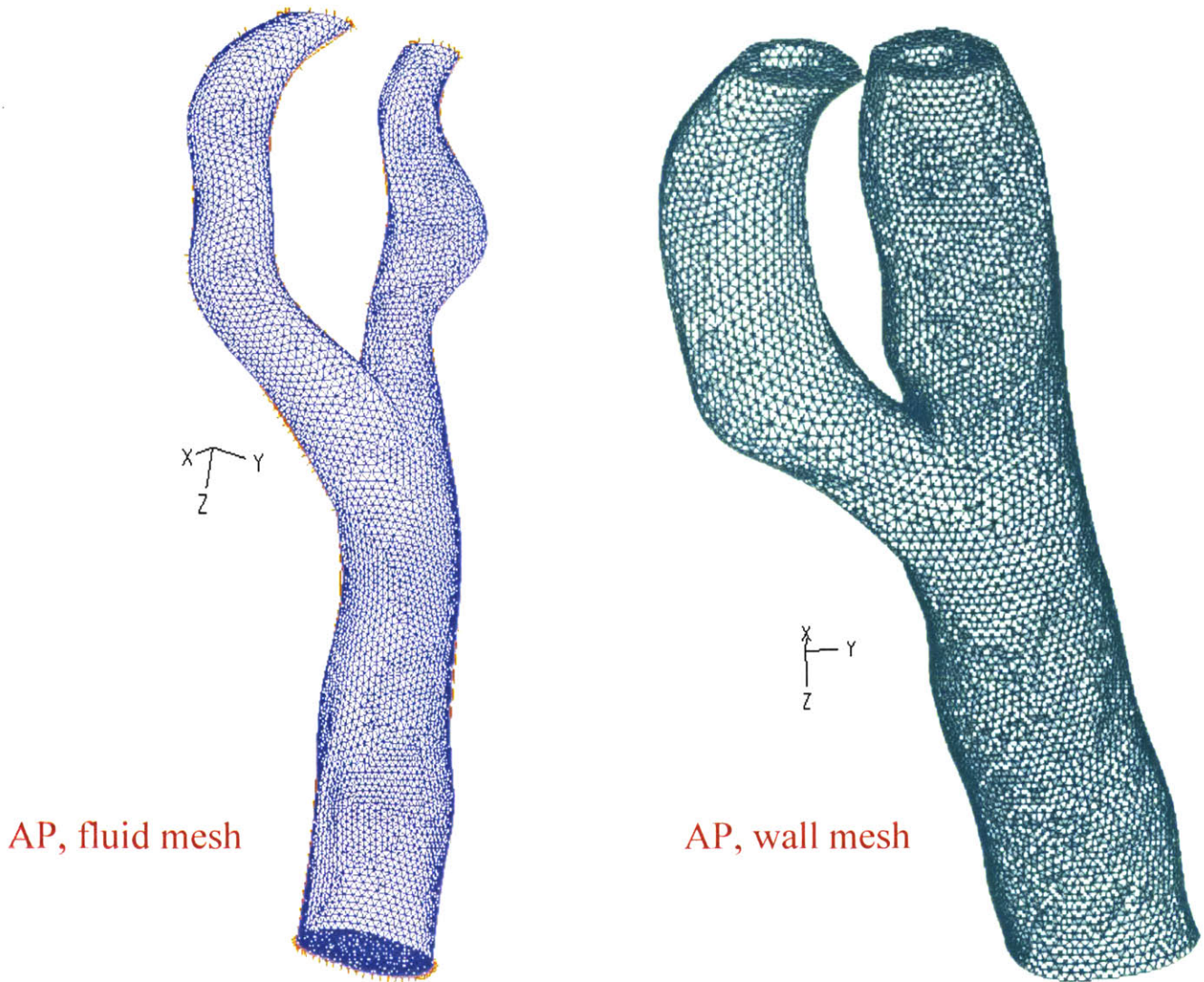


Figure 9: Fluid and wall FEM for AP

Next, the node coordinates of the fluid structure at the inlet plane to the carotid bifurcation (common carotid) and those of one of the outlet planes to the carotid bifurcation (internal carotid), are extracted and saved in a numerical matrix for later use in specifying velocity boundary conditions, described next.

#### 6. Velocity Interpolation and Construction of Time functions

In this step, a Matlab function takes as input the MR phase images containing x, y and z velocity components as a function of time, both at the inlet and outlet of carotid bifurcation. This program then outputs a numerical matrix with x, y and z velocity values



at the cartesian coordinates of the image pixels. Figure 10 shows a sample NV systolic cross-sectional velocity plot at the inlet of the carotid bifurcation.

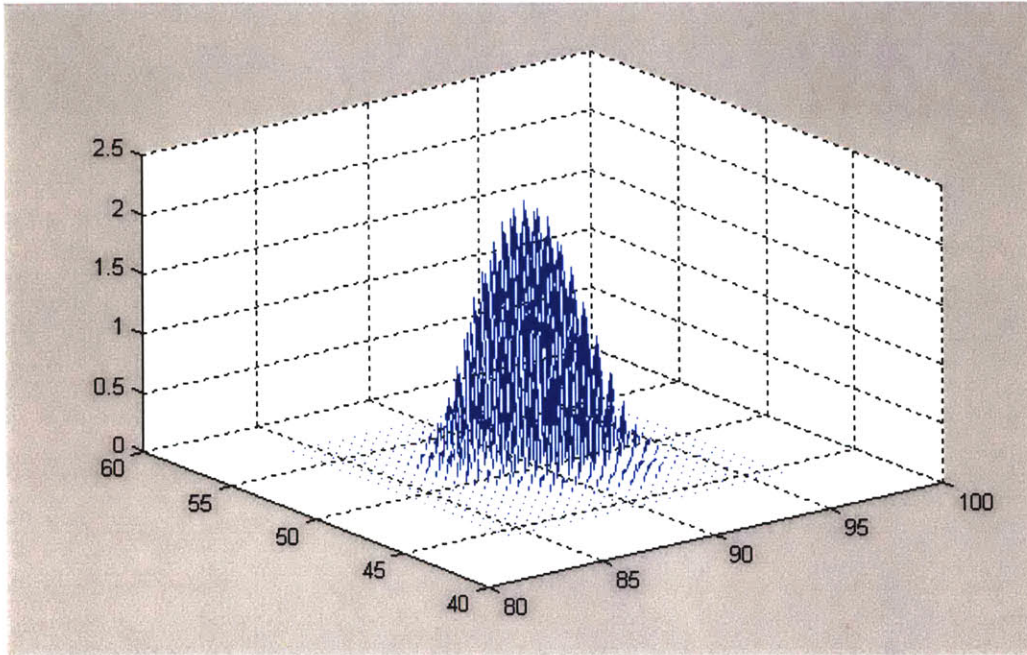


*Figure 10: NV systolic cross-sectional velocity plot at the inlet of the carotid bifurcation. The units of both axes on the horizontal plane (vessel dimensions) are mm, while those of the vertical axis (velocity) are m/s.*

Subsequently, the matrix containing the coordinates of the FEM nodes at the inlet of the fluid FEM, and that containing the velocity values at the pixel cartesian coordinates at the inlet of the fluid FEM, are inputted as arguments into a computer function in the plotting/visualization software. This function interpolates across pixel coordinates in the MR velocity data according to the inverse distance method, yielding a file with x, y and z velocity values at the cartesian coordinates of each node at the inlet of the fluid FEM. This is then repeated for the node coordinates and pixel velocity values at the outlet of the FEM fluid.

The numerical matrices obtained in this manner are then used to construct velocity time functions for the inlet and outlet cross-sections of the FEM fluid, which constitute the boundary conditions necessary to run the FEM simulation. Figure 11 shows a sample volumetric flow rate time function at the carotid bifurcation inlet plane of a NV. The time between frames is 0.078 s and the volume flow rate is in  $\text{mm}^3/\text{s}$ .

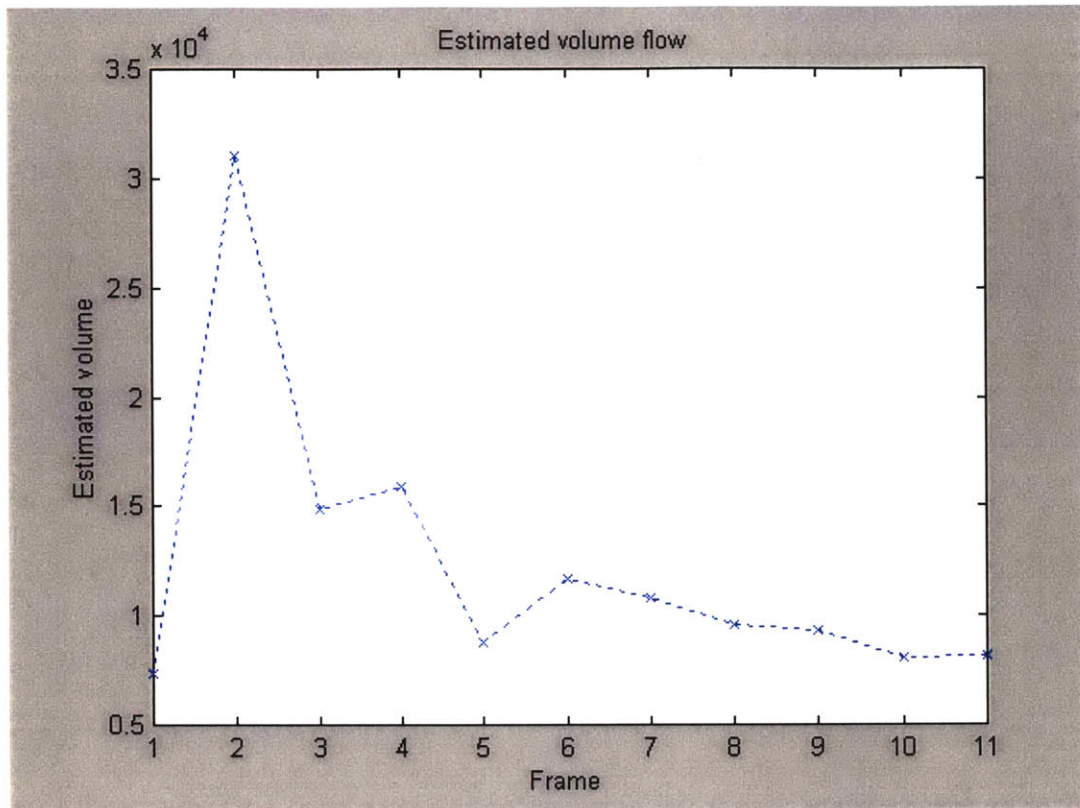


Figure 11: Volumetric flow rate time function at the carotid bifurcation inlet plane for NV. The time between frames is 0.078 s and the volume flow rate is in mm<sup>3</sup>/s.

### 7. Other specifications needed for the FEM simulation

Even though the FEM simulation is not the principal subject of this paper, it is relevant to describe some of the modeling assumptions and parameter specifications that go into the construction of the FEM simulation.

For the purpose of the FEM simulation, certain assumptions regarding the flow in the carotid bifurcation are made, and fluid and wall material properties need to be specified. The flow is assumed to be laminar, and blood is modeled as a Newtonian fluid. Regarding the material model for the wall, the artery is assumed to be isotropic and to follow the Mooney-Rivlin non-linear behavior. The strain-stiffening behavior proper of collagen fibrils is incorporated into the FEM by appropriate choice of the parameters in the Mooney-Rivlin constitutive law.

The methods described in the previous steps make it possible to run a FEM simulation of the fluid dynamics, wall mechanics and FSI of *in vivo* carotid bifurcation geometry and velocity data.

## 8. Histology: Staining

### 8.1 Rationale for choosing these four particular indicators:

Previous studies have shown that human atheroma prone to rupture, so-called vulnerable plaques, share certain geometrical and compositional characteristics. Thin fibrous cap (FC), low interstitial fibrillar collagen content of the FC (Morton, 1982), major lipid accumulation in the lesion, abundant macrophages and decreased vascular SMC's (Davies MJ, 1993), have all been shown to be recurrent features.

Macrophages participate in numerous ways at each stage of the atherosclerotic process. Continued inflammation results in increased numbers of macrophages emigrating from the blood and multiplying within the lesion. Activation of these cells leads to the release of hydrolytic enzymes, cytokines, chemokines and growth factors, which can induce further damage and eventually lead to focal necrosis (Raines, 1996). Macrophages also partake in the foam cell activation stage of atherogenesis, by taking up low-density lipoprotein (LDL). This protein is a major cause of injury to the endothelium and underlying SMC's. After LDL is modified, it must be taken up by macrophages in order to activate foam cells (Navab, 1996). Platelets adhere to macrophages, and platelet adhesion and mural thrombosis are ever-present in the initiation and development of atherosclerotic lesions (Ross, 1993). Additionally, myocardial infarctions occur as a result of uneven thinning and rupture of the FC, which takes place at the shoulders of the lesion, which is where macrophages enter, accumulate and are activated (Ross, 1999). These findings indicate that excess macrophage concentration constitutes a marker for vulnerable plaques.

The absence of fibrillar collagen correlates well with regions prone to plaque rupture and thrombosis in advanced lesions. Healthy arterial matrix consists mainly of types I and III fibrillar collagen, while the matrix in atherosclerotic lesions is mostly made up of proteoglycans, intermixed with loosely scattered collagen fibrils (Ross, 1999). This collagen degradation results from the elaboration of collagenases MMP-1, MMP-8 and MMP-13 (Galis, 1994). In this process, macrophages come into play yet again, in that activated T cells may stimulate MMP production by macrophages in the lesions, promoting plaque instability and further implicating an immune response.

In the initial stages of atherosclerosis, SMC's proliferate during the expansion of

lesions. In hypertensive patients, the high concentration of angiotensin II further enhances SMC proliferation, exacerbating the expansion of atherosclerotic lesions (Ross, 1999). However, a decreased SMC concentration constitutes an important marker for plaque vulnerability in advanced AP's. Vulnerable plaques contain relatively few SMC's in relation to macrophages (Falk, 1995; Lendon 1991). Given that SMC's are the major source of arterial interstitial collagen, the low content of SMC's in atheromatous plaque that results from impaired growth or even death of SMC's, may contribute to plaque vulnerability.

Together with the processes mentioned above, atherogenesis consists largely of the accumulation of extracellular lipids within the arterial wall (Davies MJ, 1993). SMC's migrate and proliferate, forming the FC, which surrounds a core of lipid and necrotic tissue that builds up with time. Accumulation of lipids causes further enlargement and restructuring of the lesion. At some point the artery can no longer compensate by dilation, and the lesion may intrude into the lumen and alter the blood flow (Ross, 1999). These results make high lipid content an indicator of plaque vulnerability.

### 8.2 Detailed Procedure:

Some days after the MR scan is performed on the atherosclerotic patients (AP's), a carotid endarterectomy is performed to remove the lesion. At the time of surgery, an incision is made along the internal carotid of the excised plaque specimen, at a location directly opposite to the flow divider. This cut continues along the same line onto the common carotid. This incision serves as an indicator of the relative position of different slices of the common carotid, and of the relative orientation of the internal and external carotid, once the specimen is sectioned for staining purposes.

A few hours after surgery, Galina Sukhova, PhD, a vascular histopathologist at Brigham and Womens' Hospital, receives the excised specimen, which has been preserved in cold saline, and cuts it in sections that are approximately 5 mm long. Figure 12 shows a sketch of the result of this procedure. The 5mm long sections are shown separated by red lines.

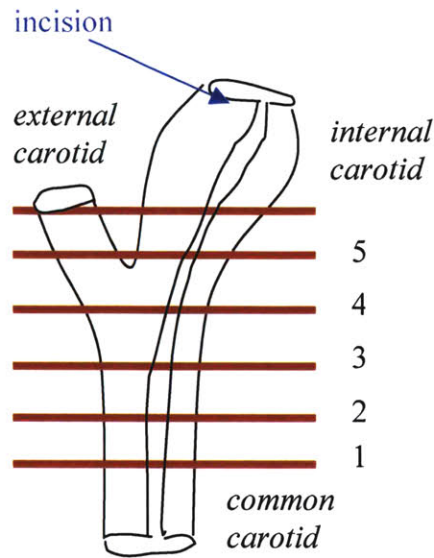


*Figure 12: Sketch of excised plaque and marker incision*

From each of these 5 mm long sections, 4 very thin slivers (each being several microns thick) are scraped, and the remaining specimen is saved. The 4 thin sections are then stained for fibrillar collagen, lipids, macrophages and SMC's, using Sirius Red, oil red o, CD68 monoclonal antibody anti-surface antigen and HHF-35 monoclonal antibody anti- $\alpha$ -actin, respectively. Figure 13 depicts a sample set of 4 stained thin sections of the excised plaque of an AP, that come from the same position of the carotid artery after the bifurcation, namely, when the common carotid has already bifurcated into the internal and external carotids.

### 9. Histology: Composition Quantification

The next step is to identify quantitatively the different components of each stained excised specimen sliver by means of image processing software. To this end, each specimen slice is photographed, and the resulting image is digitized and stored on a computer as a jpeg file.

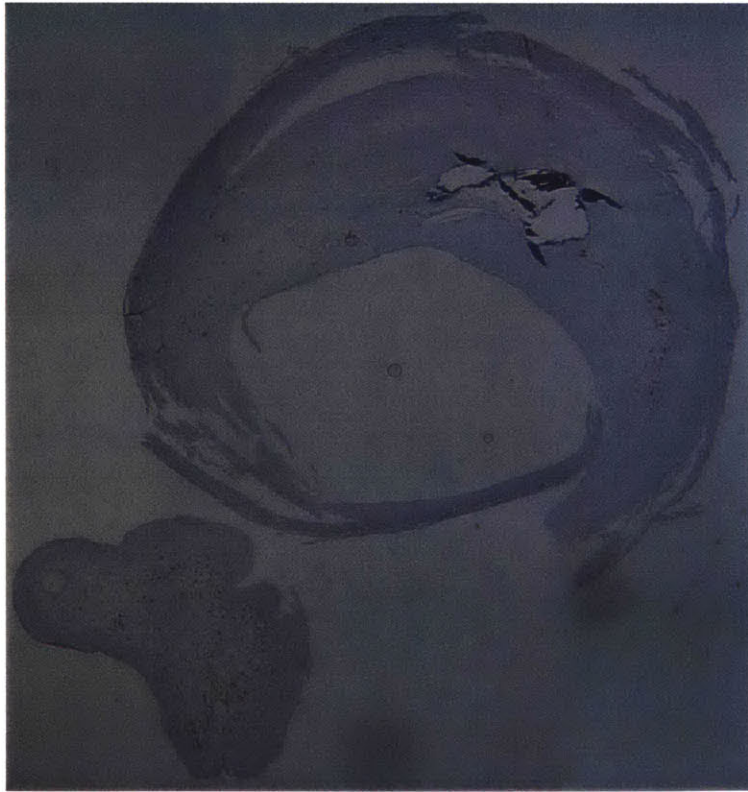
At this point, each cross sectional image is divided into 16 sectors, taken around its circumference, and analyzed to determine the percentage composition and localization of collagen, lipid, macrophage and SMC regions throughout the excised plaque. This particular way of segmenting the images was chosen for several reasons.



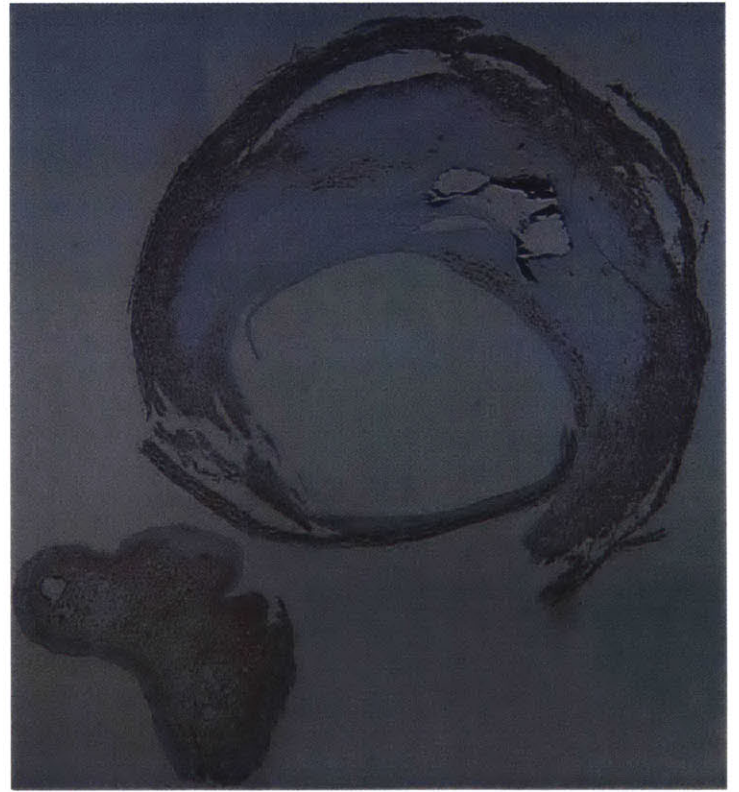
**Collagen**



**Lipids**



**Macrophages**



**SMC's**

*Figure 13: 4 stained slivers of the excised plaque of an AP from a post-bifurcation level*

Some of the critical fluid mechanic parameters that result from the FEM simulation are wall shear stress (WSS) and cyclic strain (CS). For example, given a certain longitudinal position along the carotid bifurcation (that is, at a certain z-coordinate), in order to locate points of maximum, minimum and oscillating WSS in the FEM software, one specifies several node numbers along the wall circumference. In this manner it is possible to quantify WSS as a function of the angle  $\theta$  at a certain z-position, where  $\theta$  is measured counterclockwise from the location directly opposite to the flow divider in the internal carotid, when looking at the carotid from the distal direction, for positions downstream from the flow bifurcation, and from the extrapolation of this line into the common carotid, for positions upstream from the flow divider. The center of the lumen of each artery, internal, external or common, respectively, was taken to be the origin of the coordinate system.

For the purpose of comparing WSS with the histological data, each stained jpeg image was sectioned along the circumference, and the incision was again used as the reference point from which  $\theta$  is measured. Again, the center of the lumen was set as origin. In order to reach a compromise between the level of detail in each of the stained images, and the user processing time, the number of sections into which to divide an image was limited to 16.

In a jpeg image, the color composition scheme is RGB (red, green, blue), and all staining reagents used in this study stain red. Hence, to detect the percentage composition and localization in an image of SMC's, for example, one is interested in counting every image pixel that is effectively red, and in not counting any pixel that is not red. This is accomplished in the following way: the user specifies a pixel on the image that is considered to be red to a high degree of certainty, and a threshold is selected that will mark in yellow any pixel whose red component is higher than that of the pixel which was specified. The pixels in the image that are thus marked yellow will be taken to correspond to SMC's, and the area they comprise in each of the 16 sections is calculated. The user traces out the contour of the plaque in each section and the area of plaque in each section is calculated. In a particular section, the percentage SMC area is given by the ratio of SMC to plaque area, multiplied by 100. Figure 14 shows sample sections that have been



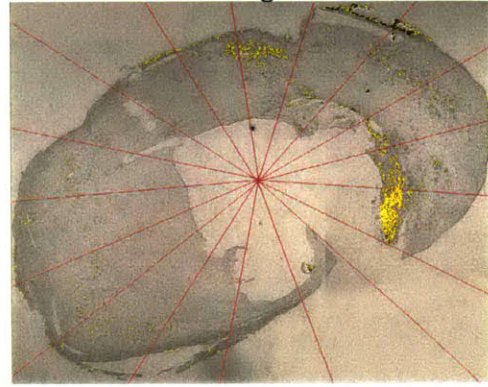
**Collagen**



**Collagen**



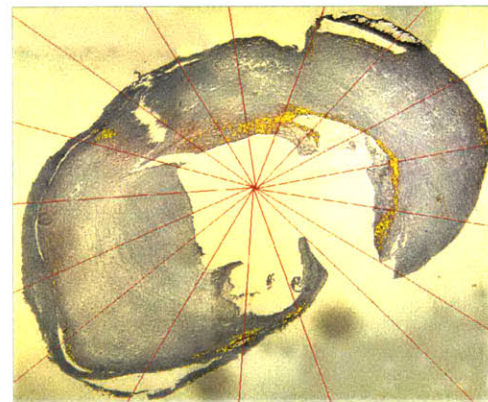
**Macrophage**



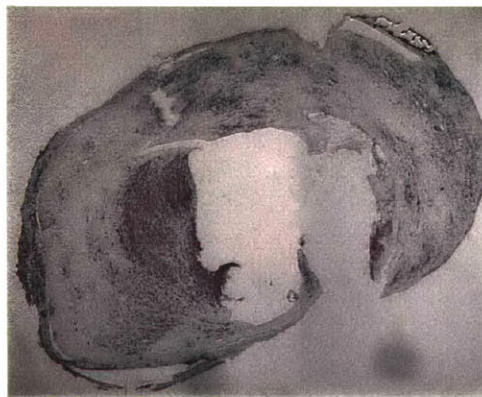
**Macrophage**



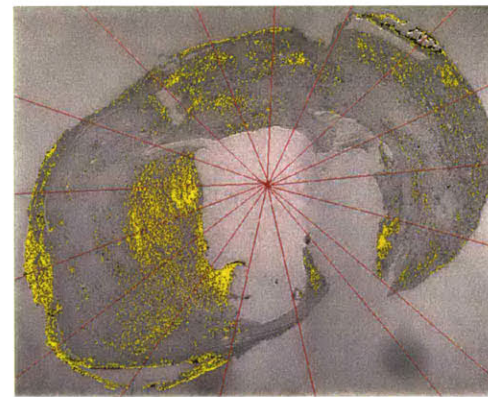
**Lipids**



**Lipids**



**SMC's**



**SMC's**

*Figure 14: Pre and post-processed images: component is marked in yellow in each case*



stained with their corresponding collagen, macrophage, lipids and SMC pixels, respectively, marked yellow, as obtained following the method described in this section.

In some images, two different parts of the specimen, that were adjacent prior to the incision, were superimposed at the time of fixing the specimen between glass slides.

Figure 15 shows an example of this event for the case of a SMC stained section.

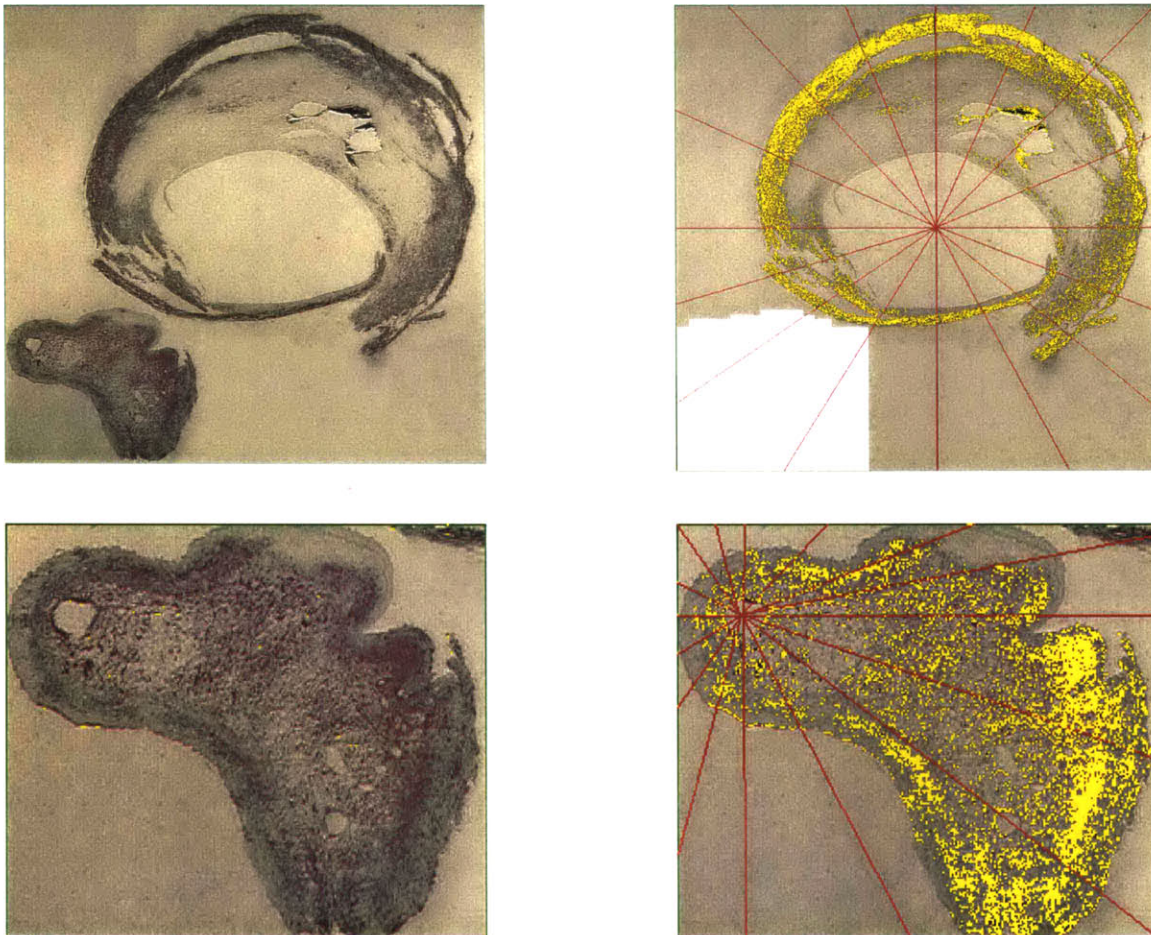


*Figure 15: Pre and post-processed image, downstream from flow division: superposition and individual quantification of external and internal carotid*

In the cases where this happened, the leading edge was set to correspond to 0 degrees, and the trailing edge to 360 degrees. In order to avoid counting pixels twice in a region that contains 2 different plaque sectors, composition quantification within a region where superposition took place happens in two stages. The user traces out the contour of the plaque in the section corresponding to the leading edge, the area of plaque is

calculated, the SMC area within the section corresponding to the leading edge is calculated and the percentage SMC area is given by the ratio of SMC to plaque area, multiplied by 100. Next, the user traces out the contour of the plaque in the section corresponding to the trailing edge, the area of plaque is calculated, the SMC area in the section corresponding to the trailing edge is calculated and the percentage SMC area is given by the ratio of SMC to plaque area, multiplied by 100.

In the case of images of sections downstream from the flow division, composition quantification was done individually for the external and internal carotids, respectively. This is also depicted in Figure 15, for the case of an SMC stained section, where the external carotid has been enlarged in the last two images to facilitate visualization.

It is very difficult to estimate how much the particular position of the external carotid with respect to the internal carotid changed during the fixing procedure, as a result of translation or rotation during the placement on the glass slide. Hence, the relative composition of the plaque in the external carotid at different z-positions can be estimated with certain precision, while the particular  $\theta$  location of high or low concentrations of a particular component cannot be determined accurately.

## 10. Summary of the overall protocol for the study

Figure 16 shows a flowchart with the chronological summary of the protocol described in sections 1 through 9.

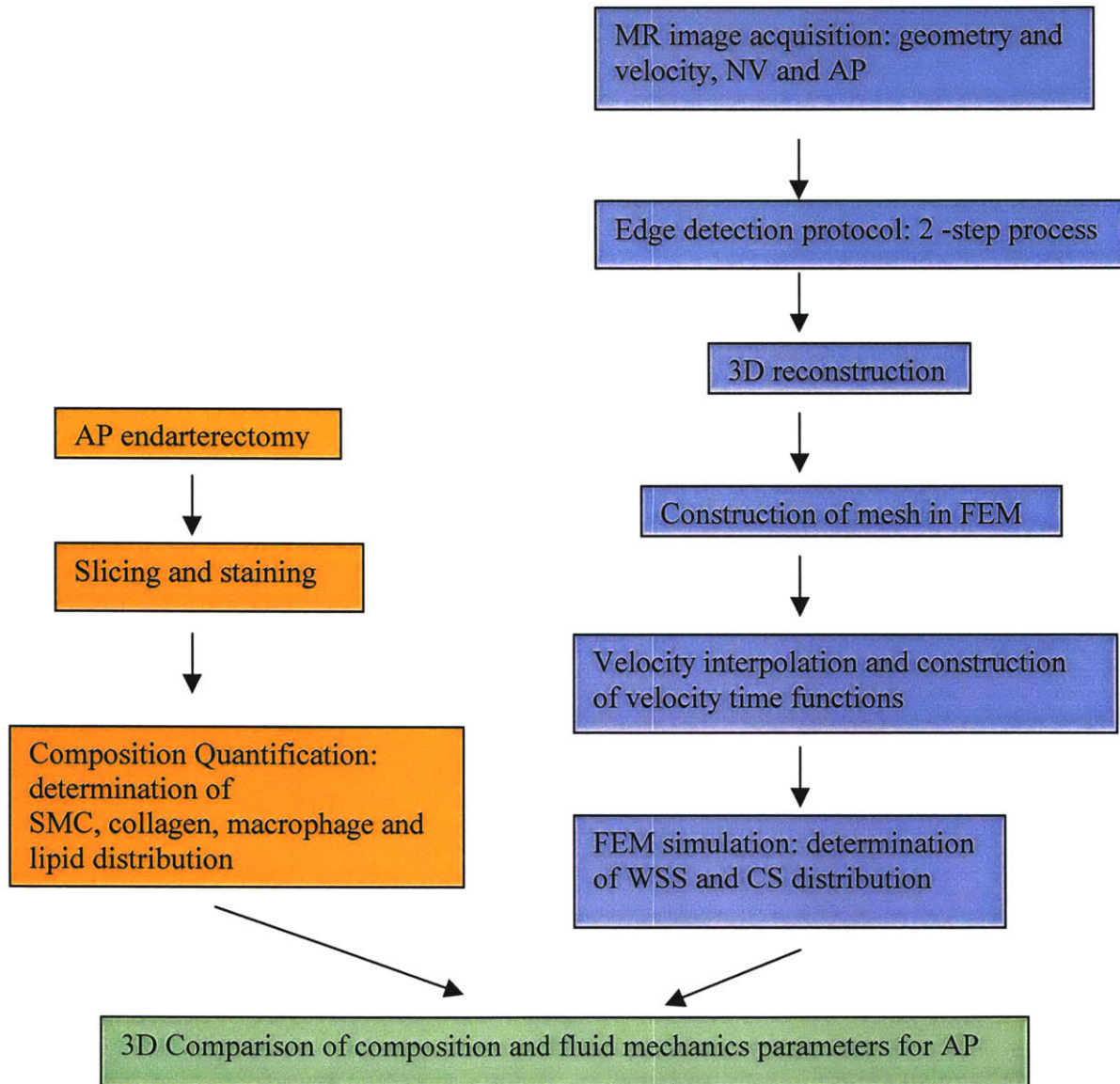


Figure 16: Protocol Flowchart

## **Discussion and Recommendations for Future Research**

### 1. Overall Strategy

Over the course of this study, there occurred several problems inherent to a multi-step study involving human subjects, different image acquisition and processing systems, as well as the coordination amongst numerous professionals from different fields, such as secretaries, surgeons, engineers, students and histopathologists. As these difficulties arose, they shaped the modifications that the initial strategy underwent, in order to improve the data acquisition and processing of the NV's and AP's that were scanned after the initial troubles.

Firstly, atherosclerotic patients who will undergo endarterectomy are, in general, elderly persons (60-80 age range). Hence, apart from atherosclerotic pathologies, they usually suffer from other ailments, such as arthritis or extremity ischemia. Consequently their lying down horizontally for long periods of time, in a restricted space such as that of a MR magnet, together with their being prevented from having any neck motion (a relatively heavy saturation pad is placed around the neck during the MR scan in order to minimize motion artifacts) can result in their experiencing numbness, back pain, and other discomforts such as claustrophobia. Hence, minimizing the length of the scanning procedure, while maintaining the highest possible degree of space and time resolution, necessary for the accurate reconstruction of the vessel geometry and the velocity functions, becomes a key objective.

Also, as different NV's were scanned, it became evident that intra-subject variability, even amongst healthy volunteers, could not be neglected. There were major differences in geometry, wall thickness, vessel orientation, and lack of symmetry among the right and left carotid bifurcation throughout the NV's that were scanned. Hence, it is vital to be very rigorous at the imaging, edge detection and 3D reconstruction stages, given that intra-subject variability is significant enough that comparison with ideal geometries, for example, when some images are blurry or missing, is in general not justified.

## 2. MR Imaging

Regarding the MR geometry and velocity images, there are several difficulties that are still in the process of being overcome. A carotid ultrasound was performed on every NV and AP that participated in the study. Ultrasound data are acquired in a continuous manner, and the velocity is measured at a unique point in space, which is, in general, taken to be close to the center of the lumen. On the other hand, MR data are acquired at many points in space in a temporally discrete manner. The ultrasound study results revealed that the MR spin-echo images consistently overestimated wall thickness, and that the MR 2D phase-contrast velocity data underestimated the peak velocities, for both NV's and AP's.

There are several distinct phenomena that could be causing the disagreements between these two imaging methods. First, a small signal to noise ratio or a small ratio of the measured velocities to the VENC, could be the reason for the seemingly low velocity values, giving systematic errors in the measured velocities. Depending on the VENC and the voxel size, there could be significant signal loss due to intravoxel dephasing. Given that in a large voxel there is a larger distribution of velocities than in a small voxel, choosing too big a voxel can cause the velocity encoding to give rise to a larger distribution of phases, which would add destructively. To reduce these effects, a smaller voxel size and a larger VENC value than those used are desirable.

Other systematic errors that might have been incurred in are those due to background phase from gradient imperfections. In a phase contrast experiment such as that used to acquire the MR velocity data, the phase difference between images is taken to generate the phase-difference image. Because the experiments are differentially flow encoded (different gradients are played out in the two experiments), gradient imperfections, such as eddy currents, will be different between the two experiments, and can result in background image phase that is completely unrelated to velocity. It is worth noting that this phase error is dependent on the orientation of the slice that is being imaged.

Additionally, acceleration errors could have occurred. The gradients that are used to encode velocity to phase will also encode acceleration and higher orders of motion to phase (such as changes in acceleration or "jerk"). The effects of acceleration will

typically be significant only with longer time of echo (TE) experiments, and with systems that have low quality (slow) gradients, given that sensitivity to higher motions grows with higher order time dependencies (such as  $TE^2$ ,  $TE^3$ , etc). TE is defined as the time from the center of the excitation pulse to the center of the echo reading. These effects can be minimized using higher receiver bandwidths or higher VENC's, both of which will reduce, unfortunately, the velocity to noise ratio.

Displacement artifacts could also be affecting the MR data. Depending on the delay between different spatial encoding steps (slice, phase and read), the moving spins will be displaced, and will thus be in different locations, and perhaps have different velocities. Once again, the best way to reduce these artifacts is to minimize TE.

Turbulence in the flow will reduce drastically the signal to noise ratio, due to intra-voxel dephasing. Due to the random nature of turbulence, it could give rise to bizarre velocity distributions. It is very difficult to counteract the impact of turbulence.

Due to the time varying nature of blood flow in the carotid bifurcation, a poor temporal resolution can result in underestimation of velocities, low pass filtering the time waveform. This effect will be spatially dependent, as the distribution of temporal frequency information is spatially dependent, and can thus affect the resulting velocity field. Hence, improving temporal resolution is likely to reduce the MR velocity data underestimation problem, although this will come at the price of a longer scanning time.

### 3. Extraction of Inner and Outer Wall coordinates and 3D Reconstruction

There is continuing work to reduce the human input into these stages of the study. This is done through the implementation of semi-automation routines that minimize user input, as well as through the unification of the 3D reconstruction steps.

### 4. Velocity Interpolation and Construction of Time functions

Examining Figure 11, which shows a sample velocity function as obtained from MR velocity data, it becomes apparent that the temporal resolution of the MR flow mapping is too low to capture some of the important transient events. If used unaltered, these would inevitably result in flow parameter inaccuracies in the FEM simulation results. Hence, the MR velocity measurements are complemented with an ultrasound

study, and these two methods are compared and integrated to produce what is taken to be the most probable velocity time function in the carotid artery.

For example, Figure 17 shows the velocity profile at the center of the lumen at a point in the mid portion of the common carotid (which corresponds approximately to the axial location of the inlet boundary condition used in this study), over the cardiac cycle, for an AP. The velocity values are in cm/s, and the spacing between tic marks, indicated by the distance between the two vertical red arrows, corresponds to an interval of one second. With this information, a velocity time function for the pixel at the center of the lumen at the inlet to the carotid bifurcation is generated. A Womersley velocity distribution is then assumed to hold across the inlet cross-section, in order to assign velocity values to the remaining pixels at this inlet boundary condition, at each point in time. At this point, the volumetric flow rate at the inlet to the carotid bifurcation as a function of time can be calculated, and compared to a graph such as that of Figure 11. Since experience shows that MR 2D phase-contrast velocity measurements consistently underestimate the actual velocity values, the velocity time function at each pixel is multiplied by a factor larger than unity, in order for the peak value during the cycle to correspond to that measured using ultrasound.

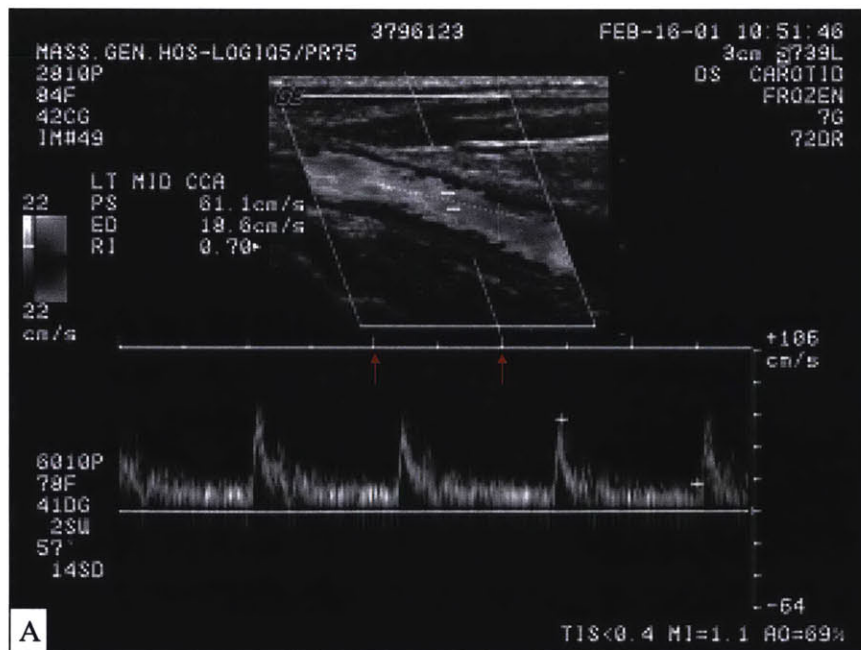


Figure 17: Velocity profile at the pixel in the center of the lumen for the mid common carotid artery (MID CCA)

Figure 18 depicts the velocity profile at the center of the lumen at a point in the distal portion of the internal carotid (which corresponds approximately to the axial location of the outlet boundary condition used in this study), over the cardiac cycle, for an AP. The procedure described above is used to generate velocity values for the remaining pixels at this outlet boundary condition, at each point in time, which are in turn used to increase the set of MR velocity values to a more plausible one.

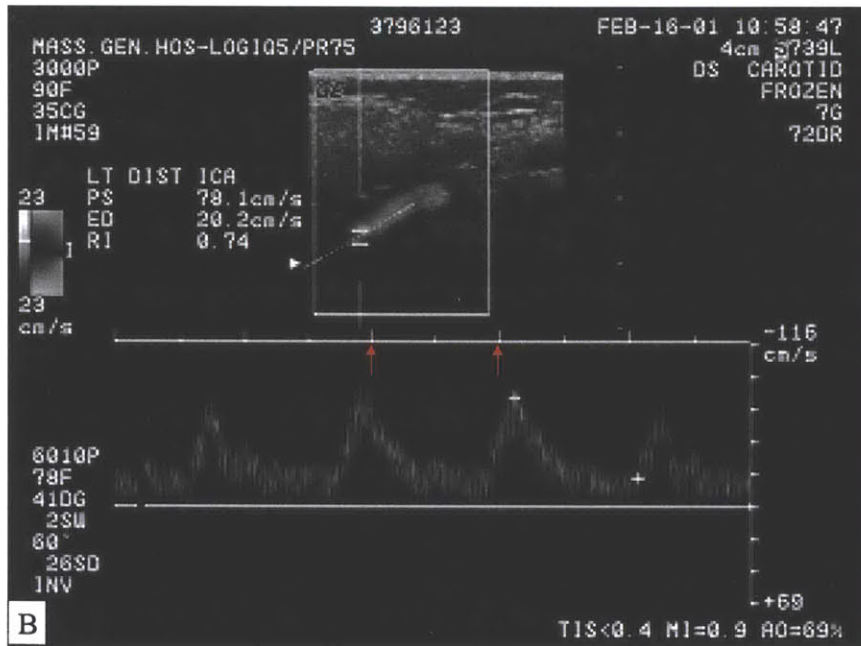


Figure 18: Velocity profile at the pixel in the center of the lumen for the mid common carotid artery (DIST ICA)

This additional carotid ultrasound requires supplementary time commitment on the part of the NV's that participate in the study, but it does not prolong that of the AP's, given that all patients that undergo carotid endarterectomy must have a carotid ultrasound performed prior to going into surgery.

## 5. Histology: Staining

It is planned to increase the number of plaque components that are stained for in this study. A qualitative and quantitative analysis of the presence of inflammatory disease markers such as tumor necrosis factor  $\alpha$  (TNF- $\alpha$ ), an indicator of primary stages of inflammation disease, and interleukin 1 $\beta$  (IL-1 $\beta$ ), an indicator of the tissue destruction



stages, are being considered. TNF- $\alpha$  and IL-1 $\beta$  are also potential mediators of MMP expression (Libby, 1995). These components are not detected in normal arteries but are expressed in atherosclerotic lesions (Sukhova, 1999). Tissue-degrading enzymes, which are thought to contribute to plaque weakening, such as MMP-1 and MMP-13, will also be stained for at a later stage in the research. Increased collagenolysis associated with macrophages has been shown to occur in high concentrations in atheromatous lesions that are more prone to rupture. Given that collagenolysis is mediated by interstitial collagenases MMP-1 and MMP-13, these constitute indicators for plaque vulnerability.

Preliminary studies have shown that preserving the geometry of individual slices and minimizing the rotation and displacement of the internal carotid relative to the external carotid, as well as the reorientation of successive slices along the carotid bifurcation, after cutting has been performed, is a key objective if it is desired to obtain a realistic 3D compositional distribution of the excised plaque.

#### 6. Histology: Composition Quantification

The method of composition quantification has several limitations and potential errors. In what refers to the division in sections, in some images, it might be difficult to determine with accuracy the center of the lumen, which is set to be the origin. In these cases, the origin offset from its actual geometric location could lead to some sections having an artificially larger or smaller total plaque area at a certain angle location, respectively. This would in turn affect the percentage composition of a particular substance in that particular section, given that the distribution of a particular component throughout the plaque is not uniform, and that the plaque area that was incorrectly counted or omitted could have a different percentage composition of a particular substance.

At the stage where the user specifies a certain pixel to be red, inconsistencies between images can be incurred in, despite it being the same user that analyzes all images. For example, a pixel with lower red composition than those chosen in other images can be specified as “red to a high degree of certainty”, increasing the relative amount of pixels whose red component is higher than that of the pixel which was specified, in that particular image.

Within a particular image, errors can be incurred in if the contour of the plaque in a particular section is traced inaccurately. For example, if the plaque contour is traced to be outside the actual contour in a particular section, the total plaque area would be overestimated, and the percentage composition of a particular substance in that particular section would be underestimated. Similarly, if this total plaque area overestimation were to happen systematically over several sections in a particular image, the percentage composition of a particular substance at a particular z coordinate would be underestimated.

In a manner similar to that related to the MR image processing stages, there is continuing work to reduce the human input into the histology quantification stage of the study. The possibility of constructing a 3D map of the excised specimen's chemical composition following steps similar to those utilized in the 3D geometry reconstruction stage is currently being explored. The Matlab code that was used in the edge detection and contour extraction step of MR images will be adapted to the histology images, in order to detect, at each axial position of the excised specimen, the external and internal boundaries, as well as the edges of regions corresponding to each particular component. This set of edges will then be used to generate a plaque geometry and composition map for each particular z-coordinate, whose coordinates can then be integrated in a unique file in order to produce a set of curves such as those in Figure 5.

Once the set of edges for each axial level is generated, it can be imported into the 3D reconstruction software, where the lofting and smoothing steps can be performed in order to produce a 3D geometry similar to that of the vessel wall in Figure 6. The geometry of this 3D composition map will be more elaborate than that of the wall in Figure 6, in that sections corresponding to different components will be indicated by different colors. This 3D composition map can then be compared to the bandplots of fluid mechanic parameters such as WSS and CS that result from the FEM simulations.

If successful, this 3D composition map generation methodology could be extended to other projects. Amongst the researchers that have shown interest in this procedure is Dr. Rich Lee, who is interested in performing 3D composition reconstruction of mouse heart histology for the Mouse Heart Project at the Brigham and Womens' Hospital.

## Conclusion

The aim of this study was to develop methods to construct a model that can be used to test, using *in vivo* MR data and stained excised plaque specimens, the hypothesis that locations on the luminal surface exposed to low fluid mechanic shear stress correlate with regions of inflammation and tissue degradation, and that sites of inflammation / degradation correlate with regions within the tissue that experience high mechanical strain.

The methods described in this thesis are successful at producing *in vivo* geometry and boundary condition data to run FEM simulations of the flow in the carotid bifurcation. Together with the fluid dynamic parameters obtained from the FEM simulations, the 3D histology composition map of the excised plaque that is currently being developed will enable to establish a correlation between tissue-borne stresses and strains, and the chemical components that are thought to correlate to atherosclerotic lesion vulnerability.

## References

- <sup>1</sup>Malek AM, Alper SL, Izumo S; Hemodynamic Shear Stress and its Role in Artherosclerosis; *JAMA*, Vol. 282, No. 21, 2035-2042, December 1, 1999.
- <sup>2</sup>Davies PF; Endothelial cells, hemodynamic forces, and the localization of atherosclerosis; Endothelial Cells, Vol. II, CRC Press, Boca Raton, FL, 123-139, 1988.
- <sup>3</sup>Field K; Matters of the heart: Interview with Dr. Anne Lees and Dr. Robert Lees; *Metro*, Brookline, May 2001.
- <sup>4</sup> Ross R; Atherosclerosis – An inflammatory disease; *N Engl J Med*, Vol. 340, No. 2, 115-126, January 1999.
- <sup>5</sup> Ross R; The pathogenesis of atherosclerosis: a perspective for the 1990's; *Nature*, Vol. 362, 801–809, 1993.
- <sup>6</sup>Davies MJ; A macro and micro view of coronary vascular insult in ischemic heart disease; *Circulation*, Vol. 82, Suppl. II, 38–46, 1990.
- <sup>7</sup>Davies PF, Tripathi SC; Mechanical Stress Mechanisms and the Cell: An Endothelial Paradigm; *Circulation Research*, Vol. 72, No. 2, 239-245, February 1993.
- <sup>8</sup>Sumpio BE; Hemodynamic forces and the biology of the endothelium: signal transduction pathways in endothelial cells subjected to physical forces in vitro; *Journal of Vascular Surgery*, Vol. 13, No. 5, 744-746, May 1991.
- <sup>9</sup>Loree HM, Kamm RD, Stringfellow RG et al; Effects of fibrous cap thickness on peak circumferential stress in model atherosclerotic vessels; *Circ Res*, Vol. 71, 850-858, 1992.

- <sup>10</sup>Sukhova GK, Schonbeck U, Rabkin E, Schoen FJ, Poole AR, Billingham RC, Libby P; Evidence for increased collagenolysis by interstitial collagenases -1 and 13- in vulnerable human atheromatous plaques; *Circulation*, Vol. 99, 2503–2509, 1999.
- <sup>11</sup>Libby P, Yeng Y-J, Aikawa M, Schoenbeck U, Mach F, Clinton SK, Sukhova GK, Lee RT; Macrophages and atherosclerotic plaque stability; *Current Opinion in Lipidology*, 330–335, 1996.
- <sup>12</sup>Lee RT, Schoen FJ, Loree HM, Lark MW, Libby P; Circumferential stress and matrix metalloproteinase 1 in human coronary atherosclerosis. Implications for plaque rupture; *Arterioscler Thromb Vasc Biol*, Vol. 16, 1070–1073, 1996.
- <sup>13</sup>Delfino A; Analysis of Stress Field in a Model of the Human Carotid Bifurcation; Physics Department, Ecole Polytechnique Federale de Lausanne, Thesis No. 1599, Lausanne, Switzerland, 1996.
- <sup>14</sup>Chan R, Kaufhold J, Lees R, Karl W; Ultrasound Analysis of vascular structure and deformation; Battlefield Biomedical Technologies II, H.H. Pien editor, Proc. SPIE, Aerosense 2000, Orlando, FL, 24-28, April 2000.
- <sup>15</sup>Shah J; A common framework for curve evolution, segmentation and anisotropic diffusion; Proc IEEE Conf. on Comp. Vis. and Patt. Recog, IEEE, xvi+932, 136-142, 1996.
- <sup>16</sup>Raines EW, Rosenfeld ME, Ross R; The role of macrophages; Fuster V, Ross R, Topol EJ, eds. Atherosclerosis and coronary artery disease, Vol. 1, Philadelphia, Lipincott-Raven, 539–555, 1996.
- <sup>17</sup>Navab M, Berliner JA, Watson AD, et al; The Yin and Yang of oxidation in the development of the fatty streak: a review based on the 1994 George Lyman Duff Memorial Lecture; *Arterioscler Thromb Vasc Biol*, Vol. 16, 831–842, 1996.

<sup>18</sup>Galis ZS, Sukhova GK, Lark MW, Libby P; Increased expression of MMP's and matrix degrading activity in vulnerable regions of human atherosclerotic plaques; *J Clin Invest*, Vol. 94, 2493–2503, 1994.

<sup>19</sup>Morton LF, Barnes MJ; Collagen polymorphism in the normal and diseased blood vessel wall: investigation of collagens type I, III and V; *Atherosclerosis*, Vol. 42, 41-51, 1982.

<sup>20</sup>Davies MJ, Richardson PD, Woolf N, Katz DR, Mann J; Risk of thrombosis in human atherosclerotic plaques: role of extracellular lipid, macrophage and smooth muscle cell content; *Br Heart J*, Vol. 69, 377–381, 1993.

<sup>21</sup>Falk E, Shah PK, Fuster V; Coronary plaque disruption; *Circulation*, Vol. 92, 657–671, 1995.

<sup>22</sup>Lendon CL, Davies MJ, Born GV, Richardson PD; Atherosclerotic plaque caps are locally weakened when macrophages density is increased; *Atherosclerosis*, Vol. 87, 87–90, 1991.

<sup>23</sup>Libby P, Sukhova G, Lee RT, Galis ZS; Cytokines regulate vascular functions related to the stability of the atherosclerotic plaque; *J Cardiovasc Pharmacol*; Vol. 25, S9–S12, 1995.